

# 2

## Governing Equations and Slip Models

In this chapter we first present the basic equations of fluid dynamics both for incompressible and compressible flows, and discuss appropriate nondimensionalizations for low-speed and high-speed flows. Although most of the flows encountered in microsystems applications are typically of low speed, micropropulsion applications may involve high-speed supersonic flows (see Section 6.6). Subsequently, we consider the compressible Navier–Stokes equations and develop a general boundary condition for velocity slip. This applies to a regime for which  $\text{Kn} < 1$ , and it corresponds to a second-order correction in Knudsen number. It improves Maxwell’s original first-order formula, which is limited to  $\text{Kn} \leq 0.1$ . The validity of this model is assessed in Chapter 4 with DSMC data, linearized Boltzmann equation solutions, as well as with experimental results. A more rigorous derivation of the governing equations from the Boltzmann equation is given in Section 15.4.2.

### 2.1 The Basic Equations of Fluid Dynamics

Consider fluid flow in the nondeformable control volume  $\Omega$  bounded by the control surface  $\partial\Omega$  with  $\mathbf{n}$  the unit outward normal. The equations of motion can then be derived in an absolute reference frame by applying the principles of mechanics and thermodynamics (Batchelor, 1998). They can be formulated in integral form for mass, momentum, and total energy,

respectively, as

$$\frac{d}{dt} \int_{\Omega} \rho d\Omega + \int_{\partial\Omega} \rho \mathbf{v} \cdot \mathbf{n} dS = 0, \quad (2.1a)$$

$$\frac{d}{dt} \int_{\Omega} \rho \mathbf{v} d\Omega + \int_{\partial\Omega} [\rho \mathbf{v}(\mathbf{v} \cdot \mathbf{n}) - \mathbf{n} \sigma] dS = \int_{\Omega} \mathbf{f} d\Omega, \quad (2.1b)$$

$$\frac{d}{dt} \int_{\Omega} E d\Omega + \int_{\partial\Omega} [E \mathbf{v} - \sigma \mathbf{v} + \mathbf{q}] \cdot \mathbf{n} dS = \int_{\Omega} \mathbf{f} \cdot \mathbf{v} d\Omega. \quad (2.1c)$$

Here  $\mathbf{v}(\mathbf{x}, t) = (u, v, w)$  is the velocity field,  $\rho$  is the density, and  $E = \rho(e + 1/2 \mathbf{v} \cdot \mathbf{v})$  is the total energy, where  $e$  represents the internal specific energy. Also,  $\sigma$  is the stress tensor,  $\mathbf{q}$  is the heat flux vector, and  $\mathbf{f}$  represents all external forces acting on this control volume. For Newtonian fluids, the stress tensor, which consists of the normal components ( $p$  for pressure) and the viscous stress tensor  $\tau$ , is a *linear* function of the velocity gradient, that is,

$$\sigma = -p\mathbf{I} + \tau, \quad (2.2a)$$

$$\tau = \mu[\nabla \mathbf{v} + (\nabla \mathbf{v})^T] + \zeta(\nabla \cdot \mathbf{v})\mathbf{I}, \quad (2.2b)$$

where  $\mathbf{I}$  is the unit tensor, and  $\mu$  and  $\zeta$  are the first (absolute) and second (bulk) coefficients of viscosity, respectively. They are related by the Stokes hypothesis, that is,  $2\mu + 3\zeta = 0$ , which expresses local thermodynamic equilibrium. (We note that the Stokes hypothesis is valid for monoatomic gases but it may not be true in general.) The heat flux vector is related to temperature gradients via the Fourier law of heat conduction, that is,

$$\mathbf{q} = -k\nabla T, \quad (2.3)$$

where  $k$  is the thermal conductivity, which may be a function of temperature  $T$ .

In the case of a *deformable control volume*, the velocity in the flux term should be recognized as in a frame of reference relative to the control surface, and the appropriate time rate of change term should be used. Considering, for example, the mass conservation equation, we have the form

$$\frac{d}{dt} \int_{\Omega} \rho d\Omega + \int_{\partial\Omega} \rho \mathbf{v}_r \cdot \mathbf{n} dS = 0,$$

or

$$\int_{\Omega} \frac{\partial \rho}{\partial t} d\Omega + \int_{\partial\Omega} \rho \mathbf{v}_r \cdot \mathbf{n} dS + \int_{\partial\Omega} \rho \mathbf{v}_{cs} \cdot \mathbf{n} dS = 0,$$

where  $\mathbf{v}_{cs}$  is the velocity of the control surface,  $\mathbf{v}_r$  is the velocity of the fluid with respect to the control surface, and the total velocity of the fluid with respect to the chosen frame is  $\mathbf{v} = \mathbf{v}_r + \mathbf{v}_{cs}$ . The above forms are equivalent, but the first expression may be more useful in applications in which the time history of the volume is of interest.

Equations (2.1a) through (2.1c) can be transformed into an equivalent set of partial differential equations by applying Gauss's theorem (assuming that sufficient conditions of differentiability exist), that is,

$$\frac{\partial \rho}{\partial t} + \nabla \cdot (\rho \mathbf{v}) = 0, \quad (2.4a)$$

$$\frac{\partial}{\partial t}(\rho \mathbf{v}) + \nabla \cdot [\rho \mathbf{v} \mathbf{v} - \boldsymbol{\sigma}] = \mathbf{f}, \quad (2.4b)$$

$$\frac{\partial}{\partial t} E + \nabla \cdot [E \mathbf{v} - \boldsymbol{\sigma} \mathbf{v} + \mathbf{q}] = \mathbf{f} \cdot \mathbf{v}. \quad (2.4c)$$

The momentum and energy equations can be rewritten in the following form by using the continuity equation (2.4a) and the constitutive equations (2.2a), (2.2b):

$$\rho \frac{D\mathbf{v}}{Dt} = -\nabla p + \nabla \cdot \boldsymbol{\tau} + \mathbf{f}, \quad (2.5a)$$

$$\rho \frac{De}{Dt} = -p \nabla \cdot \mathbf{v} - \nabla \cdot \mathbf{q} + \Phi, \quad (2.5b)$$

where  $\Phi = \boldsymbol{\tau} \cdot \nabla \mathbf{v}$  is the dissipation function and  $D/Dt = \partial/\partial t + \mathbf{v} \cdot \nabla$  is the material derivative.

In addition to the governing conservation laws, an equation of state is required. For ideal gases, it has the simple form

$$p = \rho RT, \quad (2.6)$$

where  $R$  is the ideal gas constant defined as the difference of the constant specific heats; that is,  $R = C_p - C_v$ , where  $C_v = \frac{\partial e}{\partial T}|_\rho$  and  $C_p = \gamma C_v$  with  $\gamma$  the adiabatic index. For ideal gases, the energy equation can be rewritten in terms of the temperature, since  $e = p/(\rho(\gamma - 1)) = C_v T$ , and so equation (2.5b) becomes

$$\rho C_v \frac{DT}{Dt} = -p \nabla \cdot \mathbf{v} + \nabla \cdot [k \nabla T] + \Phi. \quad (2.7)$$

The system of equations (2.4a; 2.5a), (2.6), and (2.7) is called *compressible Navier–Stokes equations*, contains six unknown variables ( $\rho, \mathbf{v}, p, T$ ) with six scalar equations. Mathematically, it is an *incomplete parabolic* system, since there are no second-order derivative terms in the continuity equation.

A hyperbolic system arises in the case of inviscid flow, that is,  $\mu = 0$  (assuming that we also neglect heat losses by thermal diffusion, that is,  $k = 0$ ). In that case we obtain the *Euler equations*, which in the absence of external forces or heat sources have the form

$$\frac{\partial \rho}{\partial t} + \nabla \cdot (\rho \mathbf{v}) = 0, \quad (2.8a)$$

$$\frac{\partial(\rho \mathbf{v})}{\partial t} + \nabla \cdot (\rho \mathbf{v} \mathbf{v}) = -\nabla p, \quad (2.8b)$$

$$\frac{\partial E}{\partial t} + \nabla \cdot [(E + p) \mathbf{v}] = 0. \quad (2.8c)$$

This system admits discontinuous solutions, and it can also describe the transition from a supersonic flow (where  $|\mathbf{v}| > c_s$ ) to subsonic flow (where  $|\mathbf{v}| < c_s$ ), where  $c_s = (\gamma RT)^{1/2}$  is the speed of sound. Typically, the transition is obtained through a shock wave, which represents a discontinuity in flow variables. In such a region the integral form of the equations should be used by analogy with equations (2.1a)–(2.1c).

### 2.1.1 Incompressible Flow

For an incompressible fluid, where  $D\rho/Dt = 0$ , the mass conservation (or continuity) equation simplifies to

$$\nabla \cdot \mathbf{v} = 0. \quad (2.9)$$

Typically, when we refer to an incompressible fluid we mean that  $\rho = \text{constant}$ , but this is not necessary for a divergence-free flow; for example, in thermal convection the density varies with temperature variations. The corresponding momentum equation has the form:

$$\rho \frac{D\mathbf{v}}{Dt} = -\nabla p + \nabla \cdot [\mu[\nabla \mathbf{v} + (\nabla \mathbf{v})^T]] + \mathbf{f}, \quad (2.10)$$

where the viscosity  $\mu(\mathbf{x}, t)$  may vary in space and time. The pressure  $p(\mathbf{x}, t)$  is not a thermodynamic quantity but can be thought of as a constraint that projects the solution  $\mathbf{v}(\mathbf{x}, t)$  onto a divergence-free space. In other words, an equation of state is no longer valid, since it will make the incompressible Navier–Stokes system overdetermined.

The acceleration terms can be written in various equivalent ways, so that in their discrete form, they conserve total linear momentum  $\int_{\Omega} \rho \mathbf{v} \, d\Omega$  and total kinetic energy  $\int_{\Omega} \rho \mathbf{v} \cdot \mathbf{v} \, d\Omega$  in the absence of viscosity and external forces. In particular, the following forms are often used:

- Convective form:  $D\mathbf{v}/Dt = \partial \mathbf{v} / \partial t + (\mathbf{v} \cdot \nabla) \mathbf{v}$ ,
- Conservative (flux) form:  $D\mathbf{v}/Dt = \partial \mathbf{v} / \partial t + \nabla \cdot (\mathbf{v} \mathbf{v})$ ,
- Rotational form:  $D\mathbf{v}/Dt = \partial \mathbf{v} / \partial t - \mathbf{v} \times (\nabla \times \mathbf{v}) + 1/2 \nabla (\mathbf{v} \cdot \mathbf{v})$ ,
- Skew-symmetric form:  $D\mathbf{v}/Dt = \partial \mathbf{v} / \partial t + 1/2 [(\mathbf{v} \cdot \nabla) \mathbf{v} + \nabla \cdot (\mathbf{v} \mathbf{v})]$ .

The incompressible Navier–Stokes equations (2.9), (2.10) are written in terms of the primitive variables  $(\mathbf{v}, p)$ . An alternative form is to rewrite these equations in terms of the velocity  $\mathbf{v}$  and vorticity  $\boldsymbol{\omega} = \nabla \times \mathbf{v}$ . This is a more general formulation than the standard vorticity-streamfunction, which is limited to two dimensions. The following system is equivalent to

equations (2.10) and (2.9), assuming that  $\rho, \mu$  are constant:

$$\rho \frac{D\boldsymbol{\omega}}{Dt} = (\boldsymbol{\omega} \cdot \nabla)\mathbf{v} + \mu \nabla^2 \boldsymbol{\omega} \quad \text{in } \Omega, \quad (2.11a)$$

$$\nabla^2 \mathbf{v} = -\nabla \times \boldsymbol{\omega} \quad \text{in } \Omega, \quad (2.11b)$$

$$\nabla \cdot \mathbf{v} = 0 \quad \text{in } \Omega, \quad (2.11c)$$

$$\boldsymbol{\omega} = \nabla \times \mathbf{v} \quad \text{in } \Omega, \quad (2.11d)$$

where the elliptic equation for the velocity  $\mathbf{v}$  is obtained using a vector identity and the divergence-free constraint. We also assume here that the domain  $\Omega$  is simply connected. An equivalent system in terms of velocity and vorticity is studied in (Karniadakis and Sherwin, 1999). The problem with the lack of direct boundary conditions for the vorticity also exists in the more often used vorticity-streamfunction formulation in two dimensions.

Finally, a note regarding **nondimensionalization**. Consider the free-stream flow  $U_0$  past a body of characteristic size  $D$  in a medium of dynamic viscosity  $\mu$  as shown in Figure 2.1. There are two characteristic time scales in the problem, the first one representing the *convective time scale*  $t_c = D/U_0$ , and the second one representing the *diffusive time scale*  $t_d = D^2/\nu$ , where  $\nu = \mu/\rho$  is the kinematic viscosity. If we nondimensionalize all lengths with  $D$ , the velocity field with  $U_0$ , and the vorticity field with  $U_0/D$ , we obtain two different nondimensional equations corresponding to the choice of the time nondimensionalization:

#### Incompressible High-Speed Flows:

$$\frac{\partial \boldsymbol{\omega}}{\partial t_c^*} + \nabla \cdot (\mathbf{v}\boldsymbol{\omega}) = (\boldsymbol{\omega} \cdot \nabla)\mathbf{v} + Re^{-1} \nabla^2 \boldsymbol{\omega},$$

#### Incompressible Low-Speed Flows:

$$\frac{\partial \boldsymbol{\omega}}{\partial t_d^*} + Re \nabla \cdot (\mathbf{v}\boldsymbol{\omega}) = Re(\boldsymbol{\omega} \cdot \nabla)\mathbf{v} + \nabla^2 \boldsymbol{\omega},$$

where  $t_c^*$  and  $t_d^*$  are the nondimensionalized time variables with respect to  $t_c$  and  $t_d$ , respectively, and  $Re = U_0 D/\nu$  is the Reynolds number. Both forms are useful in simulations, the first in high Reynolds number simulations (e.g., micronozzles, Section 6.6), and the second in low Reynolds number flows (e.g., microchannels).

In many microflow problems the nonlinear terms can be neglected, and in such cases the governing equations are the **Stokes equations**, which we can cast in the form

$$-\nu \nabla^2 \mathbf{v} + \nabla p/\rho = \mathbf{f} \quad \text{in } \Omega, \quad (2.12a)$$

$$\nabla \cdot \mathbf{v} = 0 \quad \text{in } \Omega, \quad (2.12b)$$

along with appropriate boundary conditions for  $\mathbf{v}$ .

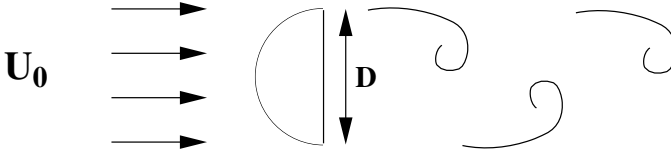


FIGURE 2.1. A schematic of free-stream flow past a microprobe in a viscous fluid.

### 2.1.2 Reduced Models

The mathematical nature of the Navier–Stokes equations varies depending on the flow that we model and the corresponding terms that dominate in the equations. For example, for an inviscid compressible flow, we obtain the Euler equations, which are of hyperbolic nature, whereas the incompressible Euler equations are of hybrid type corresponding to both real and imaginary eigenvalues. The unsteady incompressible Navier–Stokes equations are of mixed parabolic/hyperbolic nature, but the steady incompressible Navier–Stokes equations are of elliptic/parabolic type. It is instructive, especially for a reader with not much experience in fluid mechanics, to follow a hierarchical approach in reducing the Navier–Stokes equations to simpler equations so that each introduces one new concept.

Taking as an example the incompressible Navier–Stokes equations (2.9), (2.10), a simpler model is the *unsteady Stokes* system. This retains all the complexity but not the nonlinear terms; that is,

$$\begin{aligned}\frac{\partial \mathbf{v}}{\partial t} &= -\nabla p/\rho + \nu \nabla^2 \mathbf{v} + \mathbf{f} \\ \nabla \cdot \mathbf{v} &= 0.\end{aligned}$$

The Stokes system [equations (2.12a) and (2.12b)] is recovered by dropping the time derivative. Alternatively, we can drop the divergence-free constraint and study the purely parabolic scalar equation for a variable  $u$ , that is,

$$\frac{\partial u}{\partial t} = \nu \nabla^2 u + f. \quad (2.13)$$

This equation expresses unsteady diffusion and includes volumetric source terms. If we instead drop all terms on the right-hand side of (2.10), as well as the divergence-free constraint, we obtain a nonlinear advection equation. Finally, by dropping the time derivative in the parabolic equation (2.13), we obtain the **Poisson equation**,

$$-\nu \nabla^2 u = f,$$

which is encountered often in MEMS (micro electro mechanical systems), e.g., in electrostatics.

## 2.2 Compressible Flow

The flow regime for  $\text{Kn} < 0.01$  is known as the *continuum regime*, where the Navier–Stokes equations with no-slip boundary conditions govern the flow. In the *slip flow regime* ( $0.01 \leq \text{Kn} \leq 0.1$ ) the often-assumed no-slip boundary conditions seem to fail, and a sublayer on the order of one mean free path, known as the Knudsen layer, starts to become dominant between the bulk of the fluid and the wall surface. The flow, in the Knudsen layer cannot be analyzed with the Navier–Stokes equations, and it requires special solutions of the Boltzmann equation (see Section 15.4 and also (Sone, 2002)). However, for  $\text{Kn} \leq 0.1$ , the Knudsen layer covers less than 10% of the channel height (or the boundary layer thickness for external flows), and this layer can be neglected by extrapolating the bulk gas flow towards the walls. This results in a finite velocity slip value at the wall, and the corresponding flow regime is known as the *slip flow regime* (i.e.,  $0.01 \leq \text{Kn} \leq 0.1$ ). In the slip flow regime the flow is governed by the Navier–Stokes equations, and rarefaction effects are modeled through the partial slip at the wall using Maxwell’s velocity slip and von Smoluchowski’s temperature jump boundary conditions (Kennard, 1938).

For example, it may, however, be misleading to identify the flow regimes as “slip” and “continuum,” since the “no-slip” boundary condition is just an empirical finding, and the Navier–Stokes equations are valid for both the slip and the continuum flow regimes. Nevertheless, this identification was first made for rarefied gas flow research almost a century ago, and we will follow this terminology throughout this book.

In the *transition regime* ( $\text{Kn} \geq 0.1$ ) the constitutive laws that define the stress tensor and the heat flux vector break down (Chapman and Cowling, 1970), requiring higher-order corrections to the constitutive laws, resulting in the Burnett or Woods equations (Woods, 1993). It is also possible to use the Boltzmann equation directly, which is valid at the microscopic level (see Section 15.4). The Burnett and Woods equations are derived from the Boltzmann equation based on the Chapman–Enskog expansion of the velocity distribution function  $f$ , including terms up to  $\text{Kn}^2$  in the following form:

$$f = f_0(1 + a \text{Kn} + b \text{Kn}^2), \quad (2.14)$$

where  $a$  and  $b$  are functions of gas density, temperature, and macroscopic velocity vector, and  $f_0$  is the equilibrium (Maxwellian) distribution function (Chapman and Cowling, 1970):

$$f_0 = \left( \frac{m}{2\pi k_B T_0} \right)^{3/2} \exp \left( -\frac{mv^2}{2k_B T_0} \right), \quad (2.15)$$

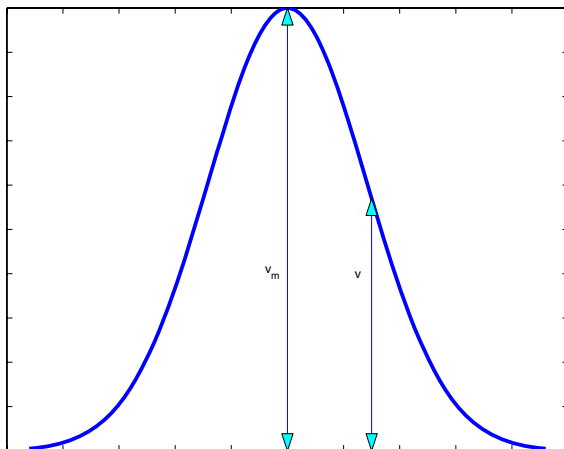


FIGURE 2.2. A plot of the Maxwellian distribution showing the most probable velocity and the mean thermal velocity, equation (2.15).

which is plotted in Figure 2.2. Here  $m$  is the molecular mass,  $k_B$  is the Boltzmann constant,  $T_0$  is the temperature, and  $v$  is the mean thermal velocity of the molecules. The zeroth-order solution of equation (2.14) is the equilibrium solution, where flow gradients vanish; i.e., the viscous stress tensor and the heat flux vector vanish, giving the Euler equations (Chapman and Cowling, 1970). Therefore,  $\text{Kn} \equiv 0$  corresponds to the Euler equations. This is a *singular limit* in transition from the Navier–Stokes equations to the Euler equations, where the infinitesimally small viscosity (or heat conduction coefficient) vanishes.

**Remark:** In this book  $\text{Kn} = 0$  is commonly used to indicate the *no-slip* flow limit, and hence in the rest of this work  $\text{Kn} = 0$  indicates a limit that  $\text{Kn} \rightarrow 0$ , but never  $\text{Kn} \equiv 0$ !

The first-order solution in  $\text{Kn}$  yields the Navier–Stokes equations, and the second-order solution in  $\text{Kn}$  yields the Burnett equations. The Woods equations have a different form in the high-order corrections of the stress tensor and heat flux terms (Woods, 1993; Welder et al., 1993).

We rewrite here equations (2.4b), (2.4c) for compressible flows in two dimensions:



$$\begin{aligned} \frac{\partial}{\partial t} \begin{pmatrix} \rho \\ \rho u_1 \\ \rho u_2 \\ E \end{pmatrix} + \frac{\partial}{\partial x_1} \begin{pmatrix} \rho u_1 \\ \rho u_1^2 + p + \sigma_{11} \\ \rho u_1 u_2 + \sigma_{12} \\ (E + p + \sigma_{11}) \cdot u_1 + \sigma_{12} \cdot u_2 + q_1 \end{pmatrix} \\ + \frac{\partial}{\partial x_2} \begin{pmatrix} \rho u_2 \\ \rho u_1 u_2 + \sigma_{21} \\ \rho u_2^2 + p + \sigma_{22} \\ (E + p + \sigma_{22}) \cdot u_2 + \sigma_{21} \cdot u_1 + q_2 \end{pmatrix} = 0, \end{aligned} \quad (2.16)$$

where the two velocity components are denoted by  $(u_1, u_2) \equiv (u, v)$  in the Cartesian coordinate system  $(x_1, x_2) \equiv (x, y)$ .

**Remark:** The conservation equations (2.16) are valid for continuum as well as for rarefied flows. However, the viscous stresses  $(\sigma_{ij})$  and the heat flux  $(q_i)$  have to be determined differently for different flow regimes (see section 15.4.2). Specifically, the *thermal stresses*

$$\frac{\partial^2 T}{\partial x_i \partial x_j} - \frac{1}{3} \frac{\partial^2 T}{\partial x_k^2} \delta_{ij}$$

in the momentum equation (derived from the Boltzmann equation) are not included in the Newtonian law for fluids. Similarly, the term in the energy equation

$$\frac{\partial^2 u_i}{\partial x_j^2}$$

is not present in the Fourier law. These terms are derived in the asymptotic analysis of the Boltzmann equation in the limit of small deviation from equilibrium (Sone, 2002). For small Knudsen number flows and with  $\mathcal{O}(M) \sim \mathcal{O}(\text{Kn})$ , the thermal stress in the momentum equation can be absorbed in the pressure term. However, if the Reynolds number of the system is large or the temperature variation is not small, then the thermal stress cannot be included in the pressure term. In this case, these extra terms have to be included explicitly in the governing equations, which are different from the above compressible Navier–Stokes equations (Sone, 2002). To this end, also the work of (Myong, 1998) may be consulted. He derived thermodynamically consistent hydrodynamic models for high Knudsen number gas flows, valid uniformly for all Mach number flows and satisfying the second law of thermodynamics.

### 2.2.1 First-Order Models

By first-order models we refer to the approximation of the Boltzmann equation up to  $\mathcal{O}(Kn)$ , i.e., the compressible Navier–Stokes equations. The con-

stitutive laws from equations (2.2a) and (2.2b) are

$$\sigma_{ij}^{NS} = -\mu \left( \frac{\partial u_j}{\partial x_i} + \frac{\partial u_i}{\partial x_j} \right) + \mu \frac{2}{3} \frac{\partial u_m}{\partial x_m} \delta_{ij} - \zeta \frac{\partial u_m}{\partial x_m} \delta_{ij}, \quad (2.17)$$

where  $\mu$  and  $\zeta$  are the dynamic (first coefficient) and bulk (second coefficient) viscosities of the fluid, and  $\delta_{ij}$  is the Kronecker delta. The heat flux is determined from Fourier's law (equation (2.3)). This level of conservation equations defines the *compressible Navier–Stokes equations*.

In the *slip flow* regime, the Navier–Stokes equations (2.16), (2.17) are solved subject to the velocity slip and temperature jump boundary conditions given by

$$u_s - u_w = \frac{2 - \sigma_v}{\sigma_v} \frac{1}{\rho(2RT_w/\pi)^{1/2}} \tau_s + \frac{3 \text{Pr}(\gamma - 1)}{4 \gamma \rho RT_w} (-q_s), \quad (2.18)$$

$$T_s - T_w = \frac{2 - \sigma_T}{\sigma_T} \left[ \frac{2(\gamma - 1)}{\gamma + 1} \right] \frac{1}{R\rho(2RT_w/\pi)^{1/2}} (-q_n), \quad (2.19)$$

where  $q_n, q_s$  are the normal and tangential heat flux components to the wall. Also,  $\tau_s$  is the viscous stress component corresponding to the skin friction,  $\gamma$  is the ratio of specific heats,  $u_w$  and  $T_w$  are the reference wall velocity and temperature, respectively. Here Pr is the Prandtl number

$$\text{Pr} = \frac{C_p \mu}{k}.$$

Equation (2.19) was proposed by Maxwell in 1879. The second term in (2.19) is associated with the thermal creep (transpiration) phenomenon, which can be important in causing pressure variation along channels in the presence of tangential temperature gradients (see Section 5.1). Since the fluid motion in a rarefied gas can be started with tangential temperature variations along the surface, the momentum and energy equations are coupled through the thermal creep effects. In addition, there are other thermal stress terms that are omitted in classical gas dynamics, but they may be present in rarefied microflows, as we discuss in Section 5.1. Equation (2.19) is due to von Smoluchowski (Kennard, 1938); it models temperature jump effects. Here  $\sigma_v, \sigma_T$  **are the tangential momentum and energy accommodation coefficients**, respectively (see Section 2.2.2). After nondimensionalization with a reference velocity and temperature, the slip conditions are written as follows:

$$U_s - U_w = \frac{2 - \sigma_v}{\sigma_v} \text{Kn} \frac{\partial U_s}{\partial n} + \frac{3}{2\pi} \frac{(\gamma - 1)}{\gamma} \frac{\text{Kn}^2 \text{Re}}{\text{Ec}} \frac{\partial T}{\partial s}, \quad (2.20a)$$

$$T_s - T_w = \frac{2 - \sigma_T}{\sigma_T} \left[ \frac{2\gamma}{\gamma + 1} \right] \frac{\text{Kn}}{\text{Pr}} \frac{\partial T}{\partial n}, \quad (2.20b)$$

where the capital letters are used to indicate nondimensional quantities. Also,  $\mathbf{n}$  and  $\mathbf{s}$  denote the outward normal (unit) vector and the tangential (unit) vector.

**Remark:** Note that while the second term on the right-hand side of equation (2.20b) (thermal creep effect) appears to be  $\mathcal{O}(\text{Kn}^2)$ , it actually corresponds to a first-order expansion (in  $\text{Kn}$ ) of the Boltzmann equation. So both velocity jump and thermal creep are derived from an  $\mathcal{O}(\text{Kn})$  asymptotic expansion of the Boltzmann equation (Sone, 2002).

To determine fully the momentum and energy transport in microdomains, we need the following nondimensional numbers:

- *Reynolds number:*  $\text{Re} = \frac{\rho u h}{\mu}$ ,
- *Eckert number:*  $\text{Ec} = \frac{u^2}{C_p \Delta T}$ , and
- *Knudsen number:*  $\text{Kn} = \frac{\lambda}{h}$ .

However, it is possible to introduce a functional relation for Knudsen number and Eckert number in terms of the Mach number

$$M = \frac{u}{\sqrt{\gamma R T_0}}.$$

The Knudsen number can be written in terms of the Mach number and Reynolds number as

$$\text{Kn} = \frac{\mu}{h \rho (2RT_w/\pi)^{1/2}} = \sqrt{\pi\gamma/2} \frac{M}{\text{Re}}, \quad (2.21)$$

while the Eckert number can be written as

$$\text{Ec} = (\gamma - 1) \frac{T_0}{\Delta T} M^2, \quad (2.22)$$

where  $\Delta T$  is a specified temperature difference in the domain, and  $T_0$  is the reference temperature used to define the Mach number. Using these relations for  $\text{Ec}$  and  $M$ , the independent parameters of the problem are reduced to three:

- **Prandtl number Pr, Reynolds number Re, and Knudsen number Kn.**

### 2.2.2 The Role of the Accommodation Coefficients

Momentum and energy transfer between the gas molecules and the surface requires specification of interactions between the impinging gas molecules and the surface. A detailed analysis of this is quite complicated and requires complete knowledge of the scattering kernels (see Section 15.4). From the

macroscopic viewpoint, it is sufficient to know some average parameters in terms of the so-called momentum and thermal accommodation coefficients in order to describe gas–wall interactions. The **thermal accommodation coefficient** ( $\sigma_T$ ) is defined by

$$\sigma_T = \frac{dE_i - dE_r}{dE_i - dE_w}, \quad (2.23)$$

where  $dE_i$  and  $dE_r$  denote the energy fluxes of incoming and reflected molecules per unit time, respectively, and  $dE_w$  denotes the energy flux if all the incoming molecules had been reemitted with the energy flux corresponding to the surface temperature  $T_w$ . The perfect energy exchange case corresponds to  $\sigma_T = 1$ . A separate thermal accommodation coefficient can be defined for the effects of gas–surface interactions on translational, rotational, and vibrational energies of the molecules. Experimental evidence indicates that under such interactions the translational and rotational energy components are more affected compared to the vibrational energy of the molecules (Schaaf and Chambre, 1961). However, such refinements cannot be applied to macroscopic models, since the rarefaction effects are treated by solving the continuum energy equation with the temperature jump boundary condition. DSMC models (see Section 15.1) can be more flexible in employing various molecule–wall collision models for different modes of energy transfer, as we show in Section 15.4.

The **tangential momentum accommodation coefficient** ( $\sigma_v$ ) can be defined for tangential momentum exchange of gas molecules with surfaces

$$\sigma_v = \frac{\tau_i - \tau_r}{\tau_i - \tau_w}, \quad (2.24)$$

where  $\tau_i$  and  $\tau_r$  show the tangential momentum of incoming and reflected molecules, respectively, and  $\tau_w$  is the tangential momentum of reemitted molecules, corresponding to that of the surface ( $\tau_w = 0$  for stationary surfaces).

- The case of  $\sigma_v = 0$  is called **specular reflection**,

where the tangential velocity of the molecules reflected from the walls is unchanged, but the normal velocity of the molecules is reversed due to the normal momentum transfer to the wall. In this case there is no tangential momentum exchange of fluid with the wall, resulting in zero skin friction. This is a limit of *inviscid flow*, where viscous stresses are zero. Hence

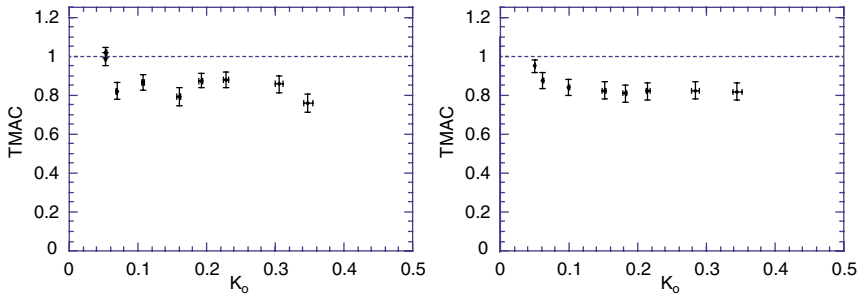
$$\frac{\partial u_s}{\partial n} \rightarrow 0 \quad \text{as} \quad \sigma_v \rightarrow 0,$$

and equation (2.20b) becomes obsolete, since the Euler equations require only the no-penetration boundary condition in this limit.

- The case of  $\sigma_v = 1$  is called **diffuse reflection**.

TABLE 2.1. Thermal and tangential momentum accommodation coefficients for typical gases and surfaces (Seidl and Steinheil, 1974; Lord, 1976).

Gas	Surface	$\sigma_T$	$\sigma_v$
Air	Al	0.87–0.97	0.87–0.97
He	Al	0.073	
Air	Iron	0.87–0.96	0.87–0.93
H <sub>2</sub>	Iron	0.31–0.55	
Air	Bronze		0.88–0.95

FIGURE 2.3. Tangential momentum accommodation coefficient  $\sigma_v$  (TMAC) versus Knudsen number obtained from mass flowrate measurements for argon (left) and for nitrogen (right). (Courtesy of K. Breuer.)

In this case the molecules are reflected from the walls with zero average tangential velocity. Therefore, the diffuse reflection is an important case for tangential momentum exchange (and thus friction) of the gas with the walls.

The tangential momentum and thermal accommodation coefficients depend on the gas and surface temperatures, local pressure, and possibly the velocity and the mean direction of the local flow. They are usually tabulated for some common gases and surfaces; see Table 2.1 and for details (Seidl and Steinheil, 1974; Lord, 1976). Diffuse reflection is likely to occur for rough surfaces. The values of  $\sigma_v$  and  $\sigma_T$  are not necessarily equal, as shown in Table 2.1. Typically, it takes a few surface collisions for a molecule to adopt the average tangential momentum of the surface, but it takes more surface collisions to obtain the energy level of the surface. Under laboratory conditions, values as low as 0.2 have been observed (Lord, 1976). Very low values of  $\sigma_v$  will increase the slip on the walls considerably even for small Knudsen number flows due to the  $(2 - \sigma)/\sigma$  factor multiplying the velocity slip and temperature jump equations.

Measurements or direct computation of accommodation coefficients are very difficult to obtain. The accommodation coefficients for microchannel flows were measured indirectly using the first-order (Arkilic et al., 2001)

and second-order slip flow theories (Maurer et al., 2003; Colin et al., 2004). Measurements of accommodation coefficients in (Arkilic et al., 2001) were obtained in the microchannel described in Chapter 1 (see Figure 1.18). Using high-resolution measurements for the mass flowrate and plotting it against the inverse pressure, the slope was computed, and based on the slip theory equations (see Chapter 4), the tangential momentum accommodation coefficient (TMAC) was obtained. The results of such measurements for argon and nitrogen are plotted in Figure 2.3 as a function of the Knudsen number. The measured value is  $\sigma_v \approx 0.80$  for nitrogen or argon or carbon dioxide in contact with prime silicon crystal in the slip and early transitional flow regime ( $0 < \text{Kn} \leq 0.4$ ). It is observed that  $\sigma_v$  is less than unity, and independent of Kn in that range (Arkilic, 1997; Arkilic et al., 2001). Lower accommodation coefficients are possible due to the low surface roughness of prime silicon crystal.

(Maurer et al., 2003) presented experimental results for helium and nitrogen flow in 1.14  $\mu\text{m}$  deep 200  $\mu\text{m}$  wide glass channel covered by an atomically flat silicon surface. Flow behavior in the slip and early transition regimes was investigated for channel-averaged Knudsen numbers of 0.8 and 0.6 for helium and nitrogen flows, respectively. Using the flowrate data and a second-order slip model represented by equation (2.42), TMAC values of  $0.91 \pm 0.03$  for helium, and  $0.87 \pm 0.06$  for nitrogen were obtained. The authors also estimated the upper limit of slip flow regime as  $\text{Kn} = 0.3 \pm 0.1$ , where Kn is based on the channel height. In a separate study, (Colin et al., 2004) presented experimental results for nitrogen and helium flow in a series of silicon microchannels fabricated using deep reactive ion etching (DRIE). Using mass flowrate and the corresponding pressure drop data, and the second-order slip model by (Deissler, 1964), they reported TMAC values of 0.93 for both helium and nitrogen. These authors reported breakdown of the first-order slip model for  $\text{Kn} \geq 0.05$ , and of the second-order theory of Deissler for  $\text{Kn} \geq 0.25$ , where Kn was based on the channel depth. These limits are unusually low compared to the values commonly accepted in the literature. A comparison between the experiments of (Colin et al., 2004) and (Maurer et al., 2003) shows that the uncertainty in the channel depth was  $\pm 0.1 \mu\text{m}$  for Colin's channels, where it was  $0.02 \mu\text{m}$  for Maurer's channels. In addition, the fabrication methods and the channel aspect ratios in these studies were different. These are certainly some of the reasons for the differences between the measurements of TMAC values by these two groups.

Finally, we note that

- *It is possible to predict the (pressure-driven) channel flowrate in the early transition flow regime, using a second-order slip solution of the Navier–Stokes equations. However, this procedure may create erroneous velocity profiles, as shown in Figures 4.11 and 4.17.*

We caution the reader about these limitations of the second-order theory

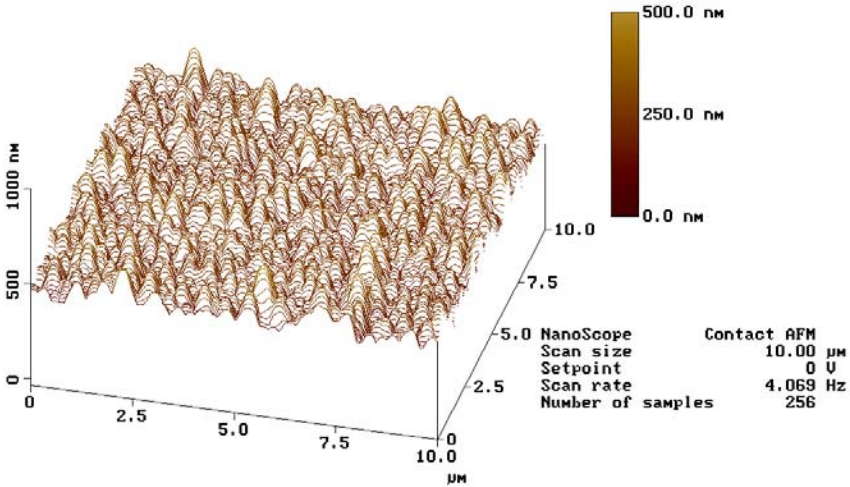


FIGURE 2.4. Profile of a polysilicon mirror surface; scan area  $10 \times 10 \mu\text{m}$ . (Courtesy of C. Liu.)

in the context of validation efforts using integral (e.g., mass flowrate versus pressure drop) measurements.

**Roughness** plays a very important role in microscales, but it is difficult to quantify its effect. In practice, it can be characterized using an atomic force microscope (AFM) for nonconductive surfaces, scanning tunnelling microscope (STM) for conductive surfaces, WYCO interferometer for optical nondestructive evaluation, and scanning electron microscope (SEM). Micron-scale roughness can be produced by wet chemical etching. A typical surface profile for a polysilicon mirror surface is shown in Figure 2.4.

The effects of roughness are difficult to analyze theoretically or numerically, but some progress has been made. (Richardson, 1973) considered a periodically modulated (rough) wall and applied a shear stress-free boundary condition. He showed analytically that the no-slip boundary condition is actually a consequence of surface roughness. In a systematic molecular dynamics study, (Mo and Rosenberger, 1990) investigated the effects of both periodic and random roughness with amplitude  $A$ . They found that as the roughness height (amplitude)  $A$  increases compared to the mean free path  $\lambda$ , the velocity slip at the wall decreases. Specifically, they proposed a criterion for the no-slip condition to be valid based on the ratio  $\lambda/A$ . If this ratio is of order unity, that is, if the roughness height is smaller but comparable to the mean free path, then the no-slip condition is satisfied. Otherwise, significant slip at the wall is present, which for atomically smooth walls occurs if the global Knudsen number, i.e., the ratio  $\lambda/h$  (with  $h$  the channel height), is finite. In summary, it was concluded that:

- For a microchannel flow with atomically **smooth** walls, if the global Knudsen number  $\text{Kn}_g = \lambda/h$  is less than 0.01, then the no-slip condition at the walls is valid ( $h$  is the channel height).
- For a microchannel flow with atomically **rough** walls, if the local Knudsen number  $\text{Kn}_l = \lambda/A$  is of order unity, then the no-slip condition at the walls is valid ( $A$  is the roughness height).
- Otherwise, in both smooth or rough walls, there is significant velocity slip at the walls.

In another study, (Li et al., 2002) considered surface roughness effects on gas flows through long microtubes. They treated the rough surface as a porous film covering an impermeable surface. In the porous film region they used the Brinkman-extended Darcy model, and they employed a high-order slip model in the core region of the microtubes. Solutions in these two different regions of the tube were combined by matching the velocity slip and the shear stress at the porous-core flow interface. This enabled derivation of expressions for the pressure distribution in microtubes, including the slip effects.

## 2.3 High-Order Models

The conservation equations (2.16) are still valid for larger deviations from the equilibrium conditions; however, the stress tensor (and heat flux vector) have to be corrected for high-order rarefaction effects. The general tensor expression of the Burnett level stress tensor is

$$\begin{aligned} \sigma_{ij}^B = & -2\mu \overline{\frac{\partial u_i}{\partial x_j}} + \frac{\mu^2}{p} \left[ \omega_1 \frac{\partial u_k}{\partial x_k} \overline{\frac{\partial u_i}{\partial x_j}} + \omega_2 \left( \frac{D}{Dt} \overline{\frac{\partial u_i}{\partial x_j}} - 2 \overline{\frac{\partial u_i}{\partial x_k} \frac{\partial u_k}{\partial x_j}} \right) \right. \\ & + \omega_3 R \overline{\frac{\partial^2 T}{\partial x_i \partial x_j}} + \omega_4 \frac{1}{\rho T} \overline{\frac{\partial p}{\partial x_i} \frac{\partial T}{\partial x_j}} + \omega_5 \overline{\frac{R}{T} \frac{\partial T}{\partial x_i} \frac{\partial T}{\partial x_j}} \\ & \left. + \omega_6 \overline{\frac{\partial u_i}{\partial x_k} \frac{\partial u_k}{\partial x_j}} \right], \end{aligned} \quad (2.25)$$

where a bar over a tensor designates a nondivergent symmetric tensor, i.e.,

$$\overline{f_{ij}} = (f_{ij} + f_{ji})/2 - \delta_{ij}/3 f_{mm}.$$

Similar expressions are valid for the heat flux  $q_i^B$  (Zhong, 1993). The coefficients  $\omega_i$  depend on the gas model and have been tabulated for hard spheres and Maxwellian gas models (Schamberg, 1947; Zhong, 1993). Since the Burnett equations are of second order in  $\text{Kn}$ , they are valid in the early transition flow regime. However, fine-grid numerical solutions of certain



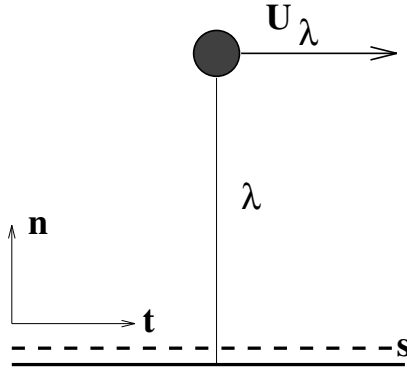


FIGURE 2.5. Control surface for tangential momentum flux near an isothermal wall moving at velocity  $U_w$ .

versions of the Burnett equations result in small wavelength instabilities. The cause of this instability has been traced to violation of the second law of thermodynamics (Balakrishnan, 2004). Using the Chapman–Enskog expansion and the Bhatnagar–Gross–Krook model of the collision integral, Balakrishnan (2004) derived the BGK–Burnett equations, and reported that the entropy-consistent behavior of the BGK–Burnett equations depends on the moment closure coefficients and approximations of the total derivative terms ( $\frac{D}{Dt}$ ) in equation (2.25). In the following we use the exact definition of the total derivative instead of the Euler approximation most commonly used in hypersonic rarefied flows (Zhong, 1993). Numerical solutions of the Burnett equations for several gas microflows can be found in (Agarwal et al., 2001; Agarwal and Yun, 2002; Xu, 2003; Lockerby and Reese, 2003; Xue et al., 2003).

Since the Burnett equations are obtained by a second-order Chapman–Enskog expansion in  $Kn$ , they require second-order slip boundary conditions. Such boundary conditions were derived by (Schamberg, 1947); however, numerical experiments with aerodynamic rarefied flows (Zhong, 1993) showed that Schamberg’s boundary conditions are inaccurate for  $Kn > 0.2$ . Similar second-order slip boundary conditions have also been proposed in (Deissler, 1964) and (Sreekanth, 1969). Detailed discussions of performance of these second-order slip models will be presented in Sections 4.1.3 and 4.2, with comparisons of the DSMC and the linearized Boltzmann results against the analytical predictions for the velocity profile.

### 2.3.1 Derivation of High-Order Slip Models

Maxwell’s derivation of equation (2.19) is based on kinetic theory. A similar boundary condition can be derived by an approximate analysis of the motion of gas in isothermal conditions. We write the tangential momentum

flux on a surface  $s$  located near the wall (see Figure 2.5) as

$$\frac{1}{4}n_s m \bar{v} u_s,$$

where  $n_s$  is the number density of the molecules crossing surface  $s$ ,  $m$  is the molecular mass,  $\bar{v}$  is the mean thermal speed defined as

$$\bar{v} = (8/\pi RT)^{0.5},$$

and  $u_s$  is the tangential (slip) velocity of the gas on this surface. If we assume that approximately half of the molecules passing through  $s$  are coming from a layer of gas at a distance proportional to one mean free path ( $\lambda = [\mu(RT\pi/2)^{1/2}/p]$ ) away from the surface, the tangential momentum flux of these incoming molecules is written as

$$\frac{1}{4}n_\lambda m \bar{v}_\lambda u_\lambda,$$

where the subscript  $\lambda$  indicates quantities evaluated one mean free path away from the surface. Since we have assumed that half of the molecules passing through  $s$  are coming from  $\lambda$  away from this surface  $n_\lambda = \frac{1}{2}n_s$ , the other half of the molecules passing through  $s$  are reflected from the wall (see Figure 2.5), and they bring to surface  $s$  a tangential momentum flux of

$$\frac{1}{4}n_w m \bar{v}_w u_r,$$

where the subscript  $w$  indicates wall conditions and the number density  $n_w$  is equal to  $\frac{1}{2}n_s$ . The average tangential velocity of the molecules reflected from the wall is shown by  $u_r$ . For determination of  $u_r$  we will use the definition of tangential momentum accommodation coefficient  $\sigma_v$ . Assuming that  $\sigma_v$  (in percentage) of the molecules are reflected from the wall *diffusely* (i.e., with average tangential velocity corresponding to that of the wall  $u_w$ ), and  $(1 - \sigma_v)$  (in percentage) of the molecules are reflected from the wall *specularly* (i.e., conserving their average incoming tangential velocity  $u_\lambda$ ), we have

$$u_r = (1 - \sigma_v)u_\lambda + \sigma_v u_w.$$

Therefore, the total tangential momentum flux on surface  $s$  is written as

$$\frac{1}{4}n_s m \bar{v} u_s = \frac{1}{4}n_\lambda m \bar{v}_\lambda u_\lambda + \frac{1}{4}n_w m \bar{v}_w [(1 - \sigma_v)u_\lambda + \sigma_v u_w].$$

Since we have assumed that the temperatures of the fluid and the surface are the same, the mean thermal speeds are identical (i.e.,  $\bar{v}_s = \bar{v}_\lambda = \bar{v}_w$ ); this is a rather strong assumption in our derivation. The number density

$n_s$  of molecules passing through the surface is composed of  $n_\lambda$  and  $n_w$ . We have assumed that  $n_\lambda = n_w = \frac{1}{2}n_s$ , which is approximately true if there is no accumulation or condensation of gas on the surface. Using the tangential momentum flux relation, the mean tangential velocity of the gas molecules on the surface, called **slip velocity**, is

$$u_s = \frac{1}{2}[u_\lambda + (1 - \sigma_v)u_\lambda + \sigma_v u_w]. \quad (2.26)$$

Schaaf and Chambre (1961) have written this expression as an average tangential velocity on a surface adjacent to an isothermal wall. Our derivation results in the same relation with approximately similar assumptions. Notice that instead of obtaining the slip information  $u_\lambda$  one mean free path away from the wall, a fraction of  $\lambda$  may be used; see (Thompson and Owens, 1975). Using a Taylor series expansion for  $u_\lambda$  about  $u_s$ , we obtain

$$u_s = \frac{1}{2} \left[ u_s + \lambda \left( \frac{\partial u}{\partial n} \right)_s + \frac{\lambda^2}{2} \left( \frac{\partial^2 u}{\partial n^2} \right)_s + \dots \right] + \frac{1}{2} \left\{ (1 - \sigma_v) \left[ u_s + \lambda \left( \frac{\partial u}{\partial n} \right)_s + \frac{\lambda^2}{2} \left( \frac{\partial^2 u}{\partial n^2} \right)_s + \dots \right] + \sigma_v \cdot u_w \right\},$$

where the normal coordinate to the wall is denoted by  $n$ . This expansion results in the following slip relation on the boundaries:

$$u_s - u_w = \frac{2 - \sigma_v}{\sigma_v} \left[ \lambda \left( \frac{\partial u}{\partial n} \right)_s + \frac{\lambda^2}{2} \left( \frac{\partial^2 u}{\partial n^2} \right)_s + \dots \right]. \quad (2.27)$$

After nondimensionalization with a reference length and velocity scale (such as free-stream velocity), we obtain

$$U_s - U_w = \frac{2 - \sigma_v}{\sigma_v} \left[ \text{Kn} \left( \frac{\partial U}{\partial n} \right)_s + \frac{\text{Kn}^2}{2} \left( \frac{\partial^2 U}{\partial n^2} \right)_s + \dots \right], \quad (2.28)$$

where we have denoted the nondimensional quantities with capital letters. By neglecting the higher-order terms in the above equation we recover Maxwell's first-order slip boundary condition (2.19) in nondimensional form. Similarly, if we truncate the above equation to include only up to second-order terms in Kn, we obtain

$$U_s - U_w = \frac{2 - \sigma_v}{\sigma_v} \left[ \text{Kn} \left( \frac{\partial U}{\partial n} \right)_s + \frac{\text{Kn}^2}{2} \left( \frac{\partial^2 U}{\partial n^2} \right)_s \right]. \quad (2.29)$$

We will use this equation for comparison of various slip models in Section 2.3.3 and in Section 4.2 .

Equation (2.26) excludes the thermal creep terms of equation (2.19), since isothermal conditions are assumed in its derivation. For nonisothermal

flows, the thermal creep effects are included to equation (2.26) separately, resulting in the following relation:

$$u_s = \frac{1}{2}[u_\lambda + (1 - \sigma_v)u_\lambda + \sigma_v u_w] + \frac{3 \text{Pr}(\gamma - 1)}{4 \gamma \rho R T_w}(-q_s).$$

For the temperature jump boundary condition, a derivation based on the kinetic theory of gases is given in (Kennard, 1938). We propose the following form for the high-order temperature jump condition by analogy with equation (2.28):

$$T_s - T_w = \frac{2 - \sigma_T}{\sigma_T} \left[ \frac{2\gamma}{\gamma + 1} \right] \frac{1}{\text{Pr}} \left[ \text{Kn} \left( \frac{\partial T}{\partial n} \right)_s + \frac{\text{Kn}^2}{2} \left( \frac{\partial^2 T}{\partial n^2} \right)_s + \frac{\text{Kn}^3}{6} \left( \frac{\partial^3 T}{\partial n^3} \right)_s + \dots \right], \quad (2.30)$$

which can be rearranged by recognizing the Taylor series expansion of  $T_\lambda$  about  $T_s$  to give a bf temperature jump boundary condition similar to equation (2.26) as

$$T_s = \left( \frac{(2 - \sigma_T)}{\text{Pr}} \frac{2\gamma}{(\gamma + 1)} T_\lambda + \sigma_T T_w \right) / \left( \sigma_T + \frac{2\gamma}{(\gamma + 1)} \frac{(2 - \sigma_T)}{\text{Pr}} \right). \quad (2.31)$$

Here  $T_\lambda$  is the temperature at the edge of the Knudsen layer, i.e., one mean free path ( $\lambda$ ) away from the wall.

### 2.3.2 General Slip Condition

The expansion originally given in (Schaaf and Chambre, 1961) is of first order in Kn. However, for higher Knudsen numbers, second-order corrections to these boundary conditions may become necessary. The velocity slip near the wall is coupled with the first and second variations of the tangential velocity in the normal direction to the wall. Numerical implementation of the slip formula in this form is computationally difficult. Therefore, further simplification of (2.28) without changing the second-order dependence on Kn is desired. For this purpose we assume that the transition from no-slip flow to slip flow occurs smoothly. Thus, a regular perturbation expansion of the velocity field in terms of Kn is defined in equation (2.32) below, where the no-slip Navier–Stokes velocity field is denoted by  $U_0(\mathbf{x}, \mathbf{t})$ , and corrections to the velocity field due to different orders of Kn dependence are denoted by  $U_i(\mathbf{x}, \mathbf{t})$  ( $i = 1, 2, 3, \dots$ ). We then have

$$U = U_0 + \text{Kn} U_1 + \text{Kn}^2 U_2 + \text{Kn}^3 U_3 + \mathcal{O}(\text{Kn}^4). \quad (2.32)$$

This substitution enables us to rewrite the Navier–Stokes equations for different orders of Kn dependence in the following form:

$$\begin{aligned}
\mathcal{O}(1) : \quad & \frac{\partial \mathbf{U}_0}{\partial t} + (\mathbf{U}_0 \cdot \nabla) \mathbf{U}_0 = -\nabla P_0 + \text{Re}^{-1} \nabla^2 \mathbf{U}_0; \\
\mathcal{O}(\text{Kn}) : \quad & \frac{\partial \mathbf{U}_1}{\partial t} + (\mathbf{U}_1 \cdot \nabla) \mathbf{U}_0 + (\mathbf{U}_0 \cdot \nabla) \mathbf{U}_1 = -\nabla P_1 + \text{Re}^{-1} \nabla^2 \mathbf{U}_1; \\
\mathcal{O}(\text{Kn}^2) : \quad & \frac{\partial \mathbf{U}_2}{\partial t} + (\mathbf{U}_0 \cdot \nabla) \mathbf{U}_2 + (\mathbf{U}_2 \cdot \nabla) \mathbf{U}_0 + (\mathbf{U}_1 \cdot \nabla) \mathbf{U}_1 \\
& = -\nabla P_2 + \text{Re}^{-1} \nabla^2 \mathbf{U}_2; \\
\mathcal{O}(\text{Kn}^3) : \quad & \frac{\partial \mathbf{U}_3}{\partial t} + (\mathbf{U}_0 \cdot \nabla) \mathbf{U}_3 + (\mathbf{U}_3 \cdot \nabla) \mathbf{U}_0 + (\mathbf{U}_2 \cdot \nabla) \mathbf{U}_1 \\
& + (\mathbf{U}_1 \cdot \nabla) \mathbf{U}_2 = -\nabla P_3 + \text{Re}^{-1} \nabla^2 \mathbf{U}_3.
\end{aligned} \tag{2.33}$$

The boundary conditions for these equations are obtained similarly by substitution of the asymptotic expansion into the slip boundary condition formula:

$$\begin{aligned}
\mathcal{O}(1) : \quad & U_0|_s = U_w, \\
\mathcal{O}(\text{Kn}) : \quad & U_1|_s = \frac{2-\sigma}{\sigma} (U'_0)|_s, \\
\mathcal{O}(\text{Kn}^2) : \quad & U_2|_s = \frac{2-\sigma}{\sigma} \left( \frac{1}{2} U''_0 + U'_1 \right)|_s, \\
\mathcal{O}(\text{Kn}^3) : \quad & U_3|_s = \frac{2-\sigma}{\sigma} \left( U'_2 + \frac{1}{2} U''_1 + \frac{1}{6} U'''_0 \right)|_s,
\end{aligned} \tag{2.34}$$

where  $U'_i$ ,  $U''_i$ , and  $U'''_i$  denote first, second, and third derivatives of the  $i$ th-order tangential velocity field along the normal direction to the surface.

A possible solution methodology for slip flow with high-order boundary conditions can be the solution of the Navier–Stokes equations order by order. However, this approach is computationally expensive, and there are numerical difficulties associated with accurate calculation of higher-order derivatives of velocity near walls with an arbitrary surface curvature.

We propose a formulation where the governing equations are directly solved without an asymptotic expansion in velocity, as mentioned above. The objective is to establish a methodology to develop slip boundary conditions accurate up to the second-order terms in Kn. First, we introduce a **new slip boundary condition**

$$U_s - U_w = \frac{2-\sigma_v}{\sigma_v} \frac{\text{Kn}}{1-B(\text{Kn})} \frac{\text{Kn}}{\text{Kn}} \left( \frac{\partial U}{\partial n} \right), \tag{2.35}$$

where  $B(\text{Kn})$  is an empirical parameter to be determined. For a general choice of  $B(\text{Kn})$ , equation (2.35) is first-order accurate in Kn, provided that  $|B(\text{Kn})| < 1$ . However, for the continuum flow regime ( $\text{Kn} \rightarrow 0.0$ )

the parameter  $B(\text{Kn})$  has a definite value. This value can be used to make equation (2.35) second-order accurate in  $\text{Kn}$  for finite  $\text{Kn}$ . For the rest of the  $\text{Kn}$  values,  $B(\text{Kn})$  can be curve-fitted accurately using the solutions of corresponding numerical models (i.e., Navier–Stokes and DSMC models) for the entire  $\text{Kn}$  range ( $0.0 < \text{Kn} < \infty$ ). Equation (2.35) suggests finite corrections for slip effects for the entire  $\text{Kn}$  range, provided that  $B(\text{Kn}) \leq 0$ . It is possible to obtain the value of the parameter  $B(\text{Kn})$  for small  $\text{Kn}$ , especially for the slip flow regime, by Taylor series expansion of  $B(\text{Kn})$  about  $\text{Kn} = 0$ . We thus obtain

$$B(\text{Kn}) = B|_0 + \left. \frac{dB}{d\text{Kn}} \right|_0 \text{Kn} + \dots = b + \text{Kn} c + \dots \quad (2.36)$$

Assuming that  $|B(\text{Kn})| < 1$ , we expand equation (2.35) in geometric series, including also the expansion given in equation (2.36) for  $B(\text{Kn})$ . This results in

$$U_s - U_w = \frac{2 - \sigma_v}{\sigma_v} \text{Kn} \frac{\partial U}{\partial n} [1 + b \text{Kn} + (b^2 + c) \text{Kn}^2 + \dots]. \quad (2.37)$$

Next, we substitute the asymptotic expansion for the velocity field (equation (2.32)) to the general slip condition given above, and rearrange the terms as a function of their Knudsen number order. This results in

$$\begin{aligned} \mathcal{O}(1) : \quad U_0|_s &= U_w; & (2.38) \\ \mathcal{O}(\text{Kn}) : \quad U_1|_s &= \frac{2 - \sigma_v}{\sigma_v} (U'_0)|_s; \\ \mathcal{O}(\text{Kn}^2) : \quad U_2|_s &= \frac{2 - \sigma_v}{\sigma_v} (bU'_0 + U'_1)|_s; \\ \mathcal{O}(\text{Kn}^3) : \quad U_3|_s &= \frac{2 - \sigma_v}{\sigma_v} (U'_2 + bU'_1 + (b^2 + c)U'_0)|_s. \end{aligned}$$

Comparing these equations with the conditions obtained from the Taylor series expansion in equation (2.35) order by order, we obtain that the two representations are identical up to the first-order terms in  $\text{Kn}$ . To match the second-order terms we must choose the parameter  $b$  as

$$b = \left( \frac{1}{2} \frac{U''_0}{U'_0} \right)_s = \frac{1}{2} \left[ \frac{\left( \frac{\partial \omega}{\partial n} \right)_0}{\omega_0} \right]_s. \quad (2.39)$$

The quantities  $U'_0$  and  $U''_0$  for an arbitrary curved surface denote first and second derivatives of the tangential component of the velocity vector along the normal direction to the surface, corresponding to a *no-slip* solution.

- The parameter  $b$  in equation (2.39) is the ratio of the vorticity flux to the wall vorticity, obtained in no-slip flow conditions. The value of  $b$  for simple flows can be found analytically.

Similarly, third-order terms in  $\text{Kn}$  can be matched if  $c$  is chosen as

$$c = \frac{1}{U'_0} \left( \frac{1}{2} U''_1 + \frac{1}{6} U'''_0 - b^2 - bU'_1 \right). \quad (2.40)$$

However, the third-order-accurate slip formula is computationally more expensive, since it requires the solutions for the  $U_1$  field. We can obtain a second-order-accurate slip formula by approximating equation (2.35) as

$$U_s - U_w = \frac{2 - \sigma_v}{\sigma_v} \frac{\text{Kn}}{1 - B \text{Kn}} \frac{\partial U}{\partial n} = \frac{2 - \sigma_v}{\sigma_v} \frac{\text{Kn}}{1 - b \text{Kn}} \frac{\partial U}{\partial n} + \mathcal{O}(\text{Kn}^3), \quad (2.41)$$

where  $b$  is the high-order slip coefficient given in equation (2.39). The error for equation (2.41) is  $\mathcal{O}(\text{Kn}^3)$ , i.e.,

$$\text{Error} = c U'_0 \text{Kn}^3.$$

Truncated geometric series containing only  $\mathcal{O}(\text{Kn}^2)$  terms could have also been used to implement the new second-order slip-boundary condition (see equation (2.37)). The error in this case is also  $\mathcal{O}(\text{Kn}^3)$ , and is given as

$$\text{Error}_{g.s.} = [U'_2 + bU'_1 + (b^2 + c)U'_0] \text{Kn}^3.$$

Since we do not know the magnitude of the  $U'_1$  and  $U'_2$  terms, it is difficult to decide which approach is better. However, we believe that using equation (2.41) is better, since this equation keeps the original form suggested in (2.35). Also for separated flows, equation (2.41) gives no slip at the separation or reattachment points (as predicted from the first-order slip formula), since the shear stress (therefore  $\frac{\partial U}{\partial n} = 0$ ) is zero at these points. However, the truncated geometric series (equation (2.37)) will give multiplication of infinitesimally small wall shear stress ( $\tau_{\text{wall}} = \mu \frac{\partial U}{\partial y} \rightarrow 0.0$ ) with large  $b$  ( $b = \frac{U''_o}{2U'_o} \rightarrow \infty$ , since  $U'_o \rightarrow 0$ ). This may result in a velocity slip at the separation point based on some numerical truncation error in the calculations.

In this section we have developed various second- and higher-order slip conditions for gas microflows. We note that the Navier–Stokes equations require only the first-order slip conditions, and the second-order slip models should be used strictly for the second-order equations, such as the Burnett or Woods equations. Throughout this book we will utilize the second-order slip conditions routinely for the Navier–Stokes equations. This can be justified by the following arguments:

TABLE 2.2. Coefficients for first- and second-order slip models.

Author	$C_1$	$C_2$
Cercignani (Cercignani and Daneri, 1963)	1.1466	0.9756
Cercignani (Hadjiconstantinou, 2003a)	1.1466	0.647
Deissler (Deissler, 1964)	1.0	9/8
Schamberg (Schamberg, 1947)	1.0	$5\pi/12$
Hsia and Domoto (Hsia and Domoto, 1983)	1.0	0.5
Maxwell (Kennard, 1938)	1.0	0.0
Equation (2.29)	1.0	-0.5

- In the small Reynolds number limit, i.e.,  $\text{Re} \ll \text{Kn} \ll 1$ , asymptotic analysis of the Boltzmann equation shows that a consistent set of governing equations and boundary conditions up to  $\mathcal{O}(\text{Kn}^2)$  is the Stokes system with second-order slip boundary conditions; see Section 15.4.2 and for details (Sone, 2002; Aoki, 2001).
- Rarefaction effects both in the aforementioned limit as well as in the limit of  $\text{Re} \sim \mathcal{O}(1) \rightarrow M \sim \mathcal{O}(\text{Kn})$  come in only through the boundary condition. This has been proven rigorously using the Boltzmann equation in (Sone, 2002).
- The high-order boundary conditions proposed include Maxwell's first-order slip conditions (2.19), (2.19) as the leading-order term. Hence, these results are correct up to  $\mathcal{O}(\text{Kn})$  in the slip flow regime, irrespective of the formal order of the utilized slip conditions.
- The general boundary condition for slip (equation (2.43)) converges to a finite value for large  $\text{Kn}$ , unlike the first-order Maxwell's boundary condition.

### 2.3.3 Comparison of Slip Models

For isothermal flows with tangential momentum accommodation coefficient  $\sigma_v = 1$ , the general second-order slip condition has the *nondimensional* form

$$U_s - U_w = C_1 \text{Kn} \left( \frac{\partial U}{\partial n} \right)_s - C_2 \text{Kn}^2 \left( \frac{\partial^2 U}{\partial n^2} \right)_s, \quad (2.42)$$

where  $(\partial/\partial n)$  denotes gradients normal to the wall surface. The coefficients  $C_1$  and  $C_2$  are the slip coefficients. Typical values of the slip coefficients developed by different investigators are shown in Table 2.2.

We will apply the second-order slip boundary conditions given above for channel flows in Chapter 4 to examine their accuracy in representing the flow profile, including the velocity slip predictions. According to Srekanth



(Sreekanth, 1969), Cercignani's second-order boundary conditions should be used only for evaluating the flow states *far from the wall*, and these conditions should not be used to evaluate space integrals in regions extending close to the walls. Sreekanth reports good agreement of second-order slip boundary conditions with his experimental results for Kn as high as Kn = 1.5 (Sreekanth, 1969). However, Sreekanth used a different second-order slip coefficient ( $C_2 = 0.14$ ) than the original ones shown in Table 2.2. He also reports a change of the first slip coefficient ( $C_1$ ) from 1.00 to 1.1466 as the Knudsen number is increased. First-order boundary conditions cease to be accurate, according to Sreekanth's study, above Kn > 0.13. More recent studies also show that Maxwell's slip boundary condition breaks down around Kn = 0.15 (Piekos and Breuer, 1995).

Implementation of second-order slip boundary conditions using equation (2.29) requires obtaining the second derivative of the tangential velocity in the normal direction to the surface ( $\partial^2 U / \partial n^2$ ), which may lead to computational difficulties, especially in complex geometric configurations. To circumvent this difficulty we have proposed in the previous section the following *general* velocity slip boundary condition.

$$U_s - U_w = \frac{2 - \sigma_v}{\sigma_v} \left[ \frac{\text{Kn}}{1 - b \text{Kn}} \left( \frac{\partial U}{\partial n} \right)_s \right], \quad (2.43)$$

where  $b$  is a general slip coefficient. Notice that the value of  $b$  can be determined such that for  $|b \text{Kn}| < 1$  the geometric series obtained from the boundary condition of equation (2.43) matches exactly the second-order equation (2.29), and thus for slip flow the above boundary condition is *second-order accurate* in the Knudsen number.

An alternative way of implementing the slip boundary condition is to use equation (2.26) derived directly from the tangential momentum flux analysis. Such a boundary condition has not been tested before, so in Section 4.1.3 we will determine the region of its validity, and in particular at what distance from the wall it should be applied, i.e.,  $\lambda$  or  $C\lambda$ , where  $C \neq 1$  (see Figure 2.5 and (Thompson and Owens, 1975)).

As regards the accuracy of two velocity slip boundary conditions, i.e., equation (2.26) versus equation (2.43), we can analyze the differences for the two-dimensional pressure-driven incompressible flow between parallel plates separated by a distance  $h$  in the slip-flow regime. Assuming isothermal conditions and that the slip is given by equation (2.26), the corresponding velocity distribution is

$$U(y) = \frac{h^2}{2\mu} \frac{dP}{dx} \left[ \frac{y^2}{h^2} - \frac{y}{h} - \frac{2 - \sigma_v}{\sigma_v} (\text{Kn} - \text{Kn}^2) \right]. \quad (2.44)$$

This is identical to the results obtained using equation (2.43) up to second-

order terms in  $\text{Kn}$ , given below:

$$U(y) = \frac{h^2}{2\mu} \frac{dP}{dx} \left[ \frac{y^2}{h^2} - \frac{y}{h} - \frac{2 - \sigma_v}{\sigma_v} \frac{\text{Kn}}{1 + \text{Kn}} \right]. \quad (2.45)$$

This equivalence can be seen by expanding the last term in equation (2.45) as a geometric series expansion in terms of powers of  $\text{Kn}$ . The leading error in equation (2.45) is therefore proportional to

$$\frac{h^2}{2\mu} \left| \frac{\partial P}{\partial x} \right| \text{Kn}^3,$$

where  $h$  is the microchannel height.

**Remarks:** We summarize here observations that will aid in evaluating the proper application and limitations of the slip boundary conditions given by equations (2.42) and (2.43).

1. The first-order slip boundary condition should be used for  $\text{Kn} \leq 0.1$  flows. Since rarefaction effects gradually become important with increased  $\text{Kn}$  (regular perturbation problem), inclusion of second- and higher-order slip effects into a Navier–Stokes–based numerical model is neither mathematically nor physically inconsistent.
2. Using the high-order slip boundary conditions with the Navier–Stokes equations can lead to some physical insight. For example, using equation (2.42) for pressure-driven flows with various slip coefficients from Table 2.2 results in different velocity profile and flowrate trends. All the models in Table 2.2, with the exception of equation (2.29), result in *increased flowrate* due to the second-order slip terms. Although this is a correct trend for flowrate, the velocity distribution predicted by these models become erroneous with increased  $\text{Kn}$ , as shown in Figures 4.11 and 4.17. This indicates that *solely using the high-order slip correction in the transition flow regime is insufficient to predict the velocity profile and the flowrate simultaneously*. In Section 4.2, we address this problem by introducing a *rarefaction correction parameter* that leads to a unified flow model for pressure-driven channel and pipe flows, when combined with the *general* slip condition (equation (2.43)). The unified model predicts the correct velocity profile, flowrate, and pressure distribution in the *entire Knudsen regime* (see Section 4.2 for details).
3. Steady plane Couette flows have linear velocity profiles, which result in  $\partial^2 U / \partial n^2 = 0$ . Therefore, the high-order slip effects in equations (2.42) and (2.43) diminish for plane Couette flows. In Section 3.2, we demonstrate a generalized slip model for linear Couette flows that is valid for  $\text{Kn} \leq 12$ .

4. As a final remark, interfacial interactions between the gas and surface molecules may result in inelastic reflections, due to the long-range interaction forces between the gas and surface molecules. Consequently, the gas molecules may condense and then evaporate after a certain time. This results in deposition of a thin layer of gas molecules on the surface. Using Langmuir's theory of adsorption, Myong (2004) explained the accommodation coefficient concept, and studied velocity slip for both monatomic and diatomic molecules. He has shown that the Langmuir model recovers Maxwell's first-order slip conditions, and he also described equation (2.43) in the context of the Langmuir model (Myong, 2004).